# RPGAN: RANDOM PATHS AS A LATENT SPACE FOR GAN INTERPRETABILITY

**Anonymous authors**
Paper under double-blind review

## ABSTRACT

In this paper, we introduce Random Path Generative Adversarial Network (RPGAN) — an alternative scheme of GANs that can serve as a tool for generative model analysis. While the latent space of a typical GAN consists of input vectors, randomly sampled from the standard Gaussian distribution, the latent space of RPGAN consists of random paths in a generator network. As we show, this design allows to associate different layers of the generator with different regions of the latent space, providing their natural interpretability. With experiments on standard benchmarks, we demonstrate that RPGAN reveals several interesting insights about roles that different layers play in the image generation process. Aside from interpretability, the RPGAN model also provides competitive generation quality and allows efficient incremental learning on new data.

## 1 INTRODUCTION

Nowadays, deep generative models thrive in the machine learning community. Dominant methods of generative modeling, such as generative adversarial networks (GANs), are currently able to produce diverse photorealistic images (Brock et al., 2019; Karras et al., 2019). Being extremely popular among academicians, these methods are also a crucial component in a wide range of applications, including image editing (Isola et al., 2017; Zhu et al., 2017), super-resolution (Ledig et al., 2017), video generation (Wang et al., 2018) and many others.

Along with practical importance, a key benefit of accurate generative models is a more complete understanding of data inherent structure. The insights about the data generation process can result in both development of new machine learning techniques and advances in industrial applications. However, most of the state-of-the-art generative models employ deep multi-layer architectures, which are difficult to interpret or explain. While many works investigate interpretability of discriminative models (Zeiler & Fergus, 2014; Simonyan et al., 2013; Mahendran & Vedaldi, 2015), only a few (Chen et al., 2016; Bau et al., 2019) address the understanding of generative ones.

In this work, we propose Random Path GAN (RPGAN) — an alternative scheme of GANs that allows natural interpretability of the generator network. In traditional GAN generators, a stochastic component that influences the individual samples is a noisy input vector, typically sampled from the standard Gaussian distribution. In contrast, RPGAN generators are designed to use another source of stochasticity, which is a stochastic routing during forward pass. In a nutshell, the generator in RPGAN consists of several consequent buckets, each including several blocks. For each sample, only one random block from each bucket is activated during generation. The training of the RPGAN model can then be performed in an adversarial manner, as in traditional GANs. As a key advantage, RPGAN scheme allows to interpret different layer blocks via "hard-coding" several of them in the forward path and analyzing generated images. As we demonstrate in the experiments, RPGAN reveals several interesting findings about the image generation process. As a practical advantage, RPGAN can be efficiently updated to new data via simple adding new layer blocks, avoiding retraining the full model from scratch. As another curious finding, we observed that RPGAN allows constructing generative models without nonlinearities.

In summary, the main contributions of our paper are the following:

- We introduce RPGAN — a scheme with an alternative source of stochasticity for GANs, which currently dominate the generative models landscape. While being close to traditional

GANs in terms of generation quality, RPGAN allows natural interpretability and efficient model updates with new data.

- With extensive experiments on the standard benchmarks, we reveal several insights about image generation process. Many of our insights confirm and extend the recent findings from Bau et al. (2019).
- We open-source the PyTorch implementation of RPGAN with common generator backbones[1].

The rest of the paper is organized as follows. In Section 2 we review relevant ideas from prior art. The proposed Random Path GAN scheme is described in Section 3 and experimentally evaluated in Section 4. Section 5 concludes the paper and discusses possible directions for future work.

## 2 Related work

In this section we briefly describe connections of RPGAN to existing ideas from prior works.

**Generative adversarial networks.** GANs are currently one of the main paradigms in generative modelling. Since the seminal paper on GANs by Goodfellow et al. (2014), a plethora of alternative loss functions, architectures, normalization, and regularization techniques were developed (Kurach et al., 2019). These days the state-of-the-art GANs are able to produce high-fidelity images, often indistinguishable from real ones (Brock et al., 2019; Karras et al., 2019). In its essence, GAN consists of two networks, generator and discriminator, which are trained jointly in an adversarial manner. In the standard GAN, the generation stochasticity is provided by the input noise vector. In RPGAN, we propose an alternative source of stochasticity via using the fixed input but random routes during forward pass in the generator.

**Specific GAN architectures.** Many prior works investigated different design choices for GANs, but to the best of our knowledge, none of them explicitly aims to propose an interpretable GAN model. Hoang et al. (2018) proposes to use several independent generators to address the mode collapse problem. Chavdarova & Fleuret (2018) employs several auxiliary local generators and discriminators to improve mode coverage as well. Huang et al. (2017) uses layer-wise generators and discriminators to enforce hidden representations produced by generator layers to be similar to the corresponding representations produced by reversed classification network. Important differences of RPGAN compared to the works described above is that it uses stochastic forward routes as its latent space and does not enforce to mimic the latent space of pretrained classifiers.

**Interpretability.** While interpretability of models based on deep neural networks is an important research direction, most of existing works address the interpretability of discriminative models. These works typically aim to understand the internal representations of networks (Zeiler & Fergus, 2014; Simonyan et al., 2013; Mahendran & Vedaldi, 2015; Dosovitskiy & Brox, 2016) or explain decisions produced by the network for particular samples (Sundararajan et al., 2017; Bach et al., 2015; Simonyan et al., 2013). However, only a few works address interpretability of generative models. Probably, the closest to ours is the recent work Bau et al. (2019), which develops a technique that allows to identify the generator parts that are responsible for the generation of different objects. Meanwhile, we adopt an alternative way and propose a new scheme of GANs that allows natural interpretation by design. Nicely, some of our findings from RPGAN interpretation confirm the results from Bau et al. (2019), which provides stronger evidence about the responsibilities of different layers in the generation process.

## 3 Random Path GAN

### 3.1 Motivation

Before the formal description, we provide an intuition behind the RPGAN model. Several prior works have demonstrated that in discriminative convolutional neural networks different layers are "responsible" for different levels of abstraction (Zeiler & Fergus, 2014; Babenko et al., 2014). For

[1]`https://github.com/rpgan-ICLR2020/RPGAN`

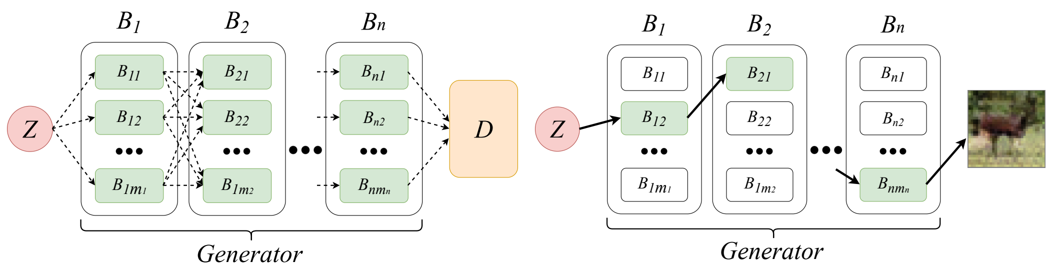

(a) Buckets formed by blocks follow by discriminator (b) Forward pass

Figure 1: RPGAN generator. On forward pass data flows only through randomly chosen blocks.

instance, earlier layers aim to detect small texture patterns, while activations in deeper layers typically correspond to semantically meaningful concepts. Similarly, in our paper we aim to understand the roles that different layers of GANs play in the image generation. Thus we propose an architecture that provides a direct way to interpret the impact of different layers. For a given generator backbone, we construct several copies of each layer in its architecture. During forward pass we randomly choose a layer instance that will be used for a particular image generation. Then to understand the RPGAN layer role, we can "freeze" a subset of layers and analyze the distribution produced by RPGAN.

## 3.2 Model

Here we formally describe the structure of the RPGAN model. The architecture is highly flexible to the choice of backbone generator and discriminator architectures as well as to loss function and learning strategy. Similarly to the standard GAN architectures, our model consists of two networks, generator and discriminator. The RPGAN discriminator operates exactly like discriminators in the existing GANs, hence below we focus on the generator description.

Unlike existing GANs, the RPGAN generator always receives a fixed input vector $Z$ during forward pass and produces an image that aims to represent real image distribution. The generator consists of several consequent *buckets* $B_1, \dots, B_n$. Each bucket is a union of independent *blocks*: $B_i{=}\{B_{i1}, \dots, B_{im_i}\}$, where each block is an arbitrary computational unit and $m_i{=}|B_i|$. A typical example of a unit can be a ResNet block (He et al., 2015), convolutional layer with nonlinearity or any other (see Figure 1a). In our experiments, all the units from the same bucket have the same architecture.

For each $i{=}1, \dots, n-1$ a block from the bucket $B_i$ produces an intermediate output tensor that is passed to a block from the next bucket $B_{i+1}$. Typically we associate each bucket with a layer (or several layers) in the backbone GAN generator architecture, which we aim to interpret or analyze. A block from the first bucket $B_1$ always receives a fixed input vector $Z$, which is the same for different forward passes. The stochasticity of the generator arises from a random path that goes from $Z$ to output, using only a single block from each bucket. Formally, during each forward pass we randomly choose indices $s_1, \dots, s_n$ with $1 \leq s_i \leq m_i$. The generator output is then computed as $B_{ns_n} \circ \cdots B_{2s_2} \circ B_{1s_1}(Z)$ (see Figure 1b). Thus, the generator defines a map from the Cartesian product $\langle m_1 \rangle \times \langle m_2 \rangle \times \cdots \times \langle m_n \rangle$ to the image space. Note that we can take an arbitrary existing GAN model, group its generator layers into buckets and replicate them into multiple blocks. In these terms, the original model can be treated as the RPGAN model with a single block in each bucket and random input noise. Note that during image generation we perform the same number of operations as in the backbone generator. Thus the inference in RPGAN has the same computational complexity as in the corresponding generator in the standard GAN.

By design, RPGAN with buckets $B_1, \dots, B_n$ and a constant input $Z$ is able to generate at most $|B_1| {\times} \cdots {\times} |B_n|$ different samples were $|B_k|$ is the number of blocks in the bucket $B_k$. Nevertheless, this number is typically much larger than a training set size and we argue that the probability space of random paths can serve as a good modeling latent space of real images distribution, as confirmed by the experiments below.

**Block diversity loss.** To guarantee that blocks in a particular bucket are different, we also add a specific diversity term in the generator loss function. The motivation of this term is to prevent blocks $B_{ki}, B_{kj}$ from learning the same weights. Let $W$ be the set of all parameters tensors of the backbone model. For each parameter $w \in W$ there is a set of parameters $\{w^{(1)}, \dots w^{(m_w)}\}$ in the RPGAN model that are copies of the original parameter stored in different blocks. We enforce blocks to have different weights by the loss term

$$-\sum_{w \in W, i \neq j} \text{MSE}\left(\frac{w^{(i)}}{s_w}, \frac{w^{(j)}}{s_w}\right)$$

Here we also normalize by the standard deviation $s_w$ of all parameters from different blocks which correspond to the same tensor of parameters in the backbone model. This normalization effectively guarantees that all buckets contribute to the diversity term.

## 4 Experiments

**Architecture.** In all the experiments we use ResNet-like generators with the spectral normalization and the hinge loss (SN-ResNet) described in Miyato et al. (2018). The blocks in the first bucket are fully-connected layers, the blocks in the last bucket are convolutional layers and blocks in all other buckets are residual blocks with two convolutions and a skip connection. If not stated otherwise, all the buckets have the same number of blocks.

**Datasets.** We performed experiments on CIFAR-10 (Krizhevsky et al., 2009), LSUN-bedroom (Yu et al., 2015) and Anime Faces (Jin et al., 2017) datasets. For different datasets we use different numbers of discriminator steps per one generator step $d_{steps}$ and number of blocks in a bucket $n_{blocks}$. We summarize the main parameters used for three datasets in Table 1. In the last column we also report *Coverage*, which is the ratio of the latent space cardinality (which equals the number of buckets power $n_{blocks}$) to the dataset size. Intuitively, large coverage guarantees that RPGAN has sufficiently rich latent space of generator routes to capture the reference dataset. In the experiments below, we demonstrate that even moderate coverage is sufficient to generate high-fidelity images (see the LSUN-bedroom dataset with coverage $\approx$ 3.3).

| Dataset | Image size | Number of buckets | $n_{blocks}$ | $d_{steps}$ | Batch size | Coverage |
|---|---|---|---|---|---|---|
| CIFAR-10 | $32 \times 32$ | 5 | 40 | 5 | 64 | 2048 |
| Anime Faces | $64 \times 64$ | 6 | 20 | 1 | 32 | $\approx 2970$ |
| LSUN-bedroom | $128 \times 128$ | 7 | 10 | 1 | 16 | $\approx 3.3$ |

Table 1: The details of architectures and training protocols used for different datasets.

**Training details.** We use the Adam optimizer with learning rate equal to $0.25 \times 10^{-3}$, $\beta_1, \beta_2$ equal to $0.5, 0.999$ and train model for $45 \times 10^4$ generator steps for CIFAR-10 and $25 \times 10^4$ generator steps for Anime faces and LSUN-bedroom datasets. During training we also optimize the unique input vector $Z$. We observed that learnable $Z$ slightly improves the final generation quality and stabilizes the learning process. During training forward pass we pass $Z$ through $N$ independent random paths. Formally, let $\{x_1, \dots, x_N\}$ be a batch of samples recieved from a bucket $B_k$. To pass this batch through the bucket $B_{k+1}$ we take random blocks $B_{ki_1}, \dots, B_{ki_N}$ and form a new batch $\{B_{ki_1}(x_1), \dots, B_{ki_N}(x_N)\}$.

### 4.1 Layers interpretation

In the first series of experiments, we aim to investigate "areas of responsibility" of different generator layers. With RPGAN architecture, we can analyze factors of variation captured by the specific block. This can be performed with a technique, schematically presented on Figure 2, for a case of a generator, consisting of five buckets. Let us aim to interpret the role of blocks from the third bucket $B_3$. Then for other buckets $B_1, B_2, B_4, B_5$ we fix arbitrary blocks, shown in blue on Figure 2. Then we can generate images corresponding to routes that contain all the fixed blocks, with the randomness coming only from varying blocks inside the target bucket $B_3$.

On Figure 3 we plot generated samples with only one "unfreezed" bucket for one image from the CIFAR-10 dataset. Intuitively, each row shows how the original generated image could change

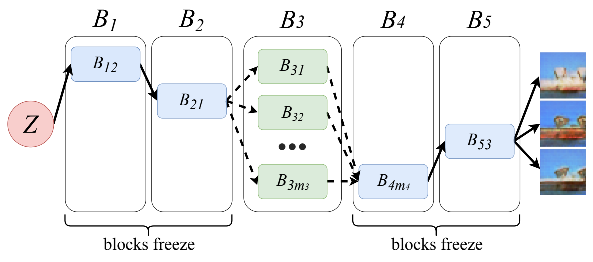

Figure 2: Five-bucket RPGAN model with fixed blocks for buckets 1, 2, 4 and 5. The only randomness comes from the bucket 3.

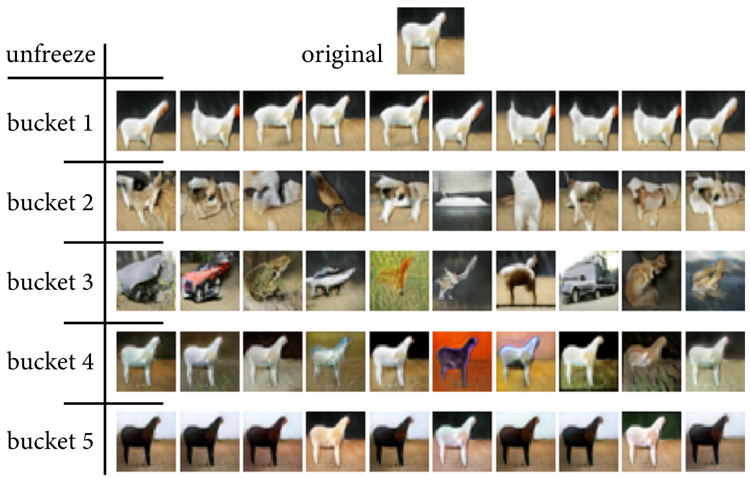

Figure 3: *Top image*: sample generated with a fixed sequence of blocks. *Horizontal lines*: samples generated by the same sequence of blocks in all buckets but one *unfreezed* bucket. In the selected bucket we choose an arbitrary block. The samples produced in this way allow to interpret factors of variation, captured by different blocks.

if we use different blocks from the corresponding bucket. Several observations from Figure 3, Figure 8, Figure 11 and Figure 14 are listed below. The first bucket typically does not influence color palette and mostly affects objects locations. The intermediate buckets have the largest influence on semantics. Meanwhile, they do not change the generated object location and general shape. The last two buckets are mostly responsible for the color scheme and do not influence the content shape. In particular, on Figure 3 the fourth layer widely varies color, while the fifth acts as a general tone corrector. Note that these findings are consistent with the insights revealed by Bau et al. (2019).

To confirm the observations quantitatively we perform the following experiment. We define a metric $d_{\mathbf{img}}$ that evaluates similarity of two generated images. Different metrics are able to capture different variations (e.g. in terms of semantic, color histogram, etc.) and we describe two particular choices of $d_{\mathbf{img}}$ below. Then we choose a random route in the RPGAN generator and for each bucket $B_l$ generate four images $s_1^{(l)}, \dots, s_4^{(l)}$, varying blocks in $B_l$. In other words, rather then take all possible pairs, we take four random samples from each line of the table in the Figure 3. Then we measure diversity w.r.t. $d_{\mathbf{img}}$ captured by bucket $B_l$ as a ratio

$$D_{l\to 1, d_{\mathbf{img}}} = \frac{\sum\limits_{i \neq j} d_{\mathbf{img}}(s_i^{(l)}, s_j^{(l)})}{\sum\limits_{i \neq j} d_{\mathbf{img}}(s_i^{(1)}, s_j^{(1)})}$$

Intuitively, we compute the relative diversity with respect to the first layer, which captured the smallest amount of variations in all the experiments. We then average these ratios over 100 independent evaluations. The high values of averaged ratio $D_{l\to 1, d_{\mathbf{img}}}$ imply higher diversity of the bucket $B_l$

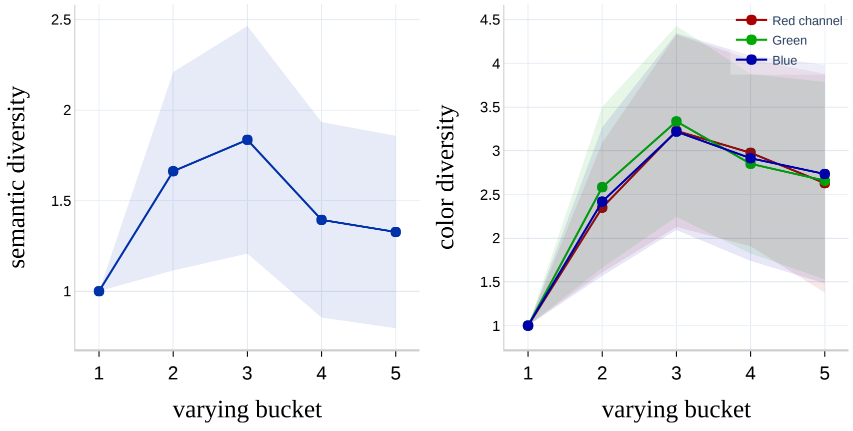

(a) Averaged relative inception impact (b) Averaged relative coloring impact

Figure 4: Layer diversity compared to the first layer on CIFAR-10.

compared to the first bucket in terms of the metric $d_{\textbf{img}}$. For $d_{\textbf{img}}$ we experimented with two following metrics, capturing semantics and color differences correspondingly.

Inspired by the well-known Fréchet Inception Score concept (Heusel et al., 2017), we use the Euclidean distance between the last layer outputs of the pretrained InceptionV3 network (Szegedy et al., 2016) for semantic distance evaluation. Namely, we define $d_{\textbf{semantic}}(img_1, img_2)$ as $\|\mathbf{Iv3}(img_1) - \mathbf{Iv3}(img_2)\|_2$ were $\mathbf{Iv3}(img)$ is the InceptionV3 model activations for image $img$.

To measure differences in color, we take the Hellinger distance between the color histograms of generated samples. Namely, for each color channel, we split the range $[0, \dots, 255]$ into $25$ equal segments and evaluate the discrete distribution defined by the frequencies the sample's pixels intensities appear in a given segment. Than the Hellinger distance between two quantified color distributions is defined as $\frac{1}{\sqrt{2}}\sqrt{\sum\limits_{i=1}^{25}(\sqrt{p_i} - \sqrt{q_i})^2}$ . We compute this metric for each color channel independently.

The average values of $D_{l \to 1, d_{\textbf{img}}}$ with the standard deviations are shown on Figure 4. It demonstrates that the semantic diversity is largest for the intermediate layers. On the contrary, the last buckets, which are closer to the output, do not influence semantics but have high impact in terms of color. Note that the first layer always shows the smallest variability in terms of both semantics and colors. The last bucket seems to be responsible for color correction and color inversion and has a lower pallet variability impact. Note, that the plots from Figure 4 reaffirm the findings coming from the Figure 3. Note that the similar empirical results also hold for other datasets (see figures 12, 15 in appendix).

Overall, we summarize the main findings common for all datasets from this experiment as:

- The earlier layer has smaller variability and seem to be responsible for the viewpoint and the position of the object on the image.
- The semantic details of the image content are mostly determined by the intermediate layers.
- The last layers typically affect only coloring scheme and do not affect content semantics or image geometry.

## 4.2 RPGAN VS BACKBONE GENERATOR

In this subsection, we argue that interpretations of different layers, obtained with RPGAN, are also valid for the standard GAN generator of the same backbone. First, we demonstrate that both standard GAN and RPGAN trained under the same training protocol provide almost the same generation quality. As the main evaluation measure, we use the Fréchet Inception Distance (FID) introduced in Heusel et al. (2017). We also compute precision-recall curve as defined in Sajjadi et al. (2018). For evaluation on CIFAR-10, we use 50.000 generated samples and the whole train dataset. We

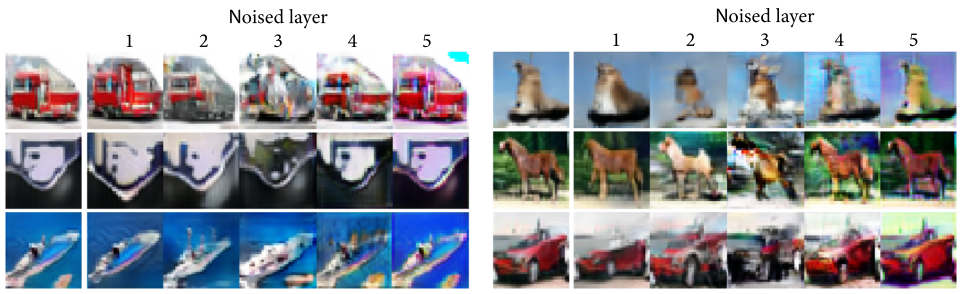

Figure 5: Images, produced by the standard SN-ResNet GAN with noise injection in the parameters of different generator layers. First column: original images, produced without parameters perturbation. Other columns: images generated with corresponding layer perturbation. Perturbations in the last two layers affects only coloring. The first layer influence mostly the object shape. The middle layers affect both coloring and details.

also take ten independently trained generators and report minimal and average FID values. See Table 2 for FID comparison and Figure 10 in appendix for precision-recall. Both in terms of FID and precision-recall curves RPGAN and SN-ResNet perform with the same quality.

| model | min FID | average FID |
|---|---|---|
| 5-buckets RPGAN | 16.9 | 20.8 |
| SN-ResNet | 16.75 | 18.7 |

Table 2: FIDs for CIFAR-10

To confirm that the layers of the standard GAN generator can be interpreted in the same way as the corresponding layers of its RPGAN counterpart, we perform the following experiment. We take a standard SN-ResNet GAN, consisting of five layers associated with the correspondent buckets in RPGAN, and train it on CIFAR-10. Then for each layer, we add a normal noise to its weights. Intuitively, we expect that the noise injection in the particular layer would change generated samples in terms of characteristics, influenced by this layer. For instance, noise in the last two layers is expected to harm coloring scheme, while noise in the intermediate layers is expected to bring maximal semantic damage. The examples of samples, produced by perturbed layers, are presented on Figure 5. The images support the intuition described above and confirm that RPGAN may serve as an analysis tool for its backbone generator model.

## 4.3 Incremental learning with RPGAN

In the next experiments, we demonstrate that the RPGAN model is also a natural fit for the generative incremental learning task (see e.g., Wu et al. (2018)). Let us assume that the whole train dataset $D$ is split into two disjoint subsets $D = D_1 \cup D_2$. Suppose that initially we have no samples from $D_2$ and trained a generative model to approximate a distribution defined by the subset $D_1$. Then, given additional samples from $D_2$, we aim to solve an incremental learning task — to update the model with new data without re-training it from scratch. The RPGAN model allows solving this task naturally. First we train a generator with buckets $B_1, \dots, B_n$ to reproduce the subset $D_1$. Once we want to extend the generator with samples from $D_2$, we add several new blocks to the buckets that are responsible for the features that capture the difference between $D_1$ and $D_2$. Then we optimize the generator to reproduce both $D_1$ and $D_2$ by training only the new blocks. Thus, instead of training a new generator from scratch, we exploit the pretrained blocks that are responsible for features, which are common for $D_1$ and $D_2$. To illustrate this scenario, we take a partition of the MNIST hand-written digits dataset (LeCun, 1989) into two subsets MNIST$_{0-6}$ and MNIST$_{7-9}$ of digits from 0 to 6 and from 7 to 9 correspondingly. As for generator for MNIST$_{0-6}$ we take a 4-bucket RPGAN model with a number of blocks equal to 20, 20, 20, 8. Note that the last bucket is much thinner than the others, as it turns out to be responsible for variations in writing style, which does not change much across the dataset. Then we train the generator on the subset MNIST$_{0-6}$ of first 7 digits (see Figure 6, left and center). After that we add five additional blocks to each of the first two layers,

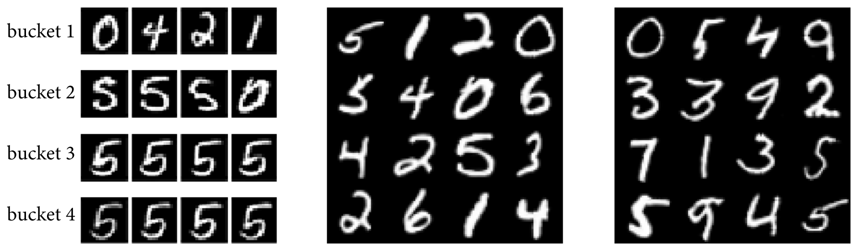

Figure 6: Incremental learning with RPGAN. *Left:* variations captured by different buckets with generator trained on MNIST$_{0-6}$. *Center:* samples picked from a generator trained on MNIST$_{0-6}$. *Right*: samples picked from a generator tuned on MNIST with only ten new blocks training (see details in the main text).

obtaining a generator with a number of blocks equal to 25, 25, 20, 8 and pretrained weights in all blocks but five in the first and in the second buckets. Then we train the extended model to fit the whole MNIST by optimizing only the new ten blocks (see Figure 6, right).

### 4.4 Purely linear generator

As a surprising side effect of our model, we discovered that decent generation quality can be achieved by the RPGAN generator **with no nonlinearities**, i.e., one can train the RPGAN generator with all blocks consisting of linear transformations only. To demonstrate that, we take an RPGAN with the same ResNet-like backbone architecture as in the experiments above. Then we replace all nonlinearities in the generator model by identity operations and train it on the CIFAR-10 dataset. The model demonstrates FID equal to 22.79 that is competitive to the state-of-the-art generative models of comparable sizes (see Figure 17 for generated images examples). Note that this approach fails for a standard GAN generator that maps a Gaussian distribution to an images distribution. Indeed, that generator would be a linear operator from a latent space to the images space with a Gaussian distribution in the images domain.

This purely linear generator architecture allows us to significantly speed up the image generation process for fully-connected layers. We group consequent buckets of fully-connected layers to form a new bucket. Blocks in the new bucket are linear transformations that are products of the blocks from the original buckets. To demonstrate this we train a fully-connected generator network on the MNIST dataset (see Table 3 in appendix, left column). Then we join the last three buckets into a single one. We form a new bucket by blocks defined by the linear operators $B_{5k} \circ B_{4j} \circ B_{3i}$ where $i, j, k$ are random indices of blocks from the buckets $B_3, B_4, B_5$ of the original generator. Thus instead of performing three multiplications of features vector from the second layer by matrices of the shapes $256 \times 512, 512 \times 1024, 1024 \times 784$ we perform a single multiplication by a $256 \times 784$ matrix. In our experiments, we achieved $\times 2.2$ speed up. Note, however, that after the compression the latent space cardinality can decrease if only a subset of tuples $(i, j, k)$ is used to populate the new bucket. Nevertheless, as random products of jointing buckets are used, we expect that the generated images would be uniformly distributed in the space of images, produced by uncompressed generator (see Figure 18 for samples comparison).

## 5 Conclusion

In this paper, we address the interpretability of generative models. In particular, we have introduced RPGAN, an alternative design of generative adversarial networks, which allows natural interpretation of different generator layers. With experiments on several datasets, we provide evidence that different layers are responsible for the different factor of variations in generated images, which is consistent with findings from previous work. As a possible direction of future research, one can more extensively use the RPGAN analysis to construct efficient models, e.g., via identification of redundant parts of the generator for pruning or inference speedup.

## REFERENCES

Artem Babenko, Anton Slesarev, Alexandr Chigorin, and Victor Lempitsky. Neural codes for image retrieval. In *European conference on computer vision*, pp. 584–599. Springer, 2014.

Sebastian Bach, Alexander Binder, Grégoire Montavon, Frederick Klauschen, Klaus-Robert Müller, and Wojciech Samek. On pixel-wise explanations for non-linear classifier decisions by layer-wise relevance propagation. *PloS one*, 10(7):e0130140, 2015.

David Bau, Jun-Yan Zhu, Hendrik Strobelt, Zhou Bolei, Joshua B. Tenenbaum, William T. Freeman, and Antonio Torralba. Gan dissection: Visualizing and understanding generative adversarial networks. In *Proceedings of the International Conference on Learning Representations (ICLR)*, 2019.

Andrew Brock, Jeff Donahue, and Karen Simonyan. Large scale GAN training for high fidelity natural image synthesis. In *International Conference on Learning Representations*, 2019. URL `https://openreview.net/forum?id=B1xsqj09Fm`.

Tatjana Chavdarova and Franois Fleuret. Sgan: An alternative training of generative adversarial networks. In *The IEEE Conference on Computer Vision and Pattern Recognition (CVPR)*, June 2018.

Xi Chen, Yan Duan, Rein Houthooft, John Schulman, Ilya Sutskever, and Pieter Abbeel. Infogan: Interpretable representation learning by information maximizing generative adversarial nets. In *Advances in neural information processing systems*, pp. 2172–2180, 2016.

Alexey Dosovitskiy and Thomas Brox. Generating images with perceptual similarity metrics based on deep networks. In *Advances in neural information processing systems*, pp. 658–666, 2016.

Ian Goodfellow, Jean Pouget-Abadie, Mehdi Mirza, Bing Xu, David Warde-Farley, Sherjil Ozair, Aaron Courville, and Yoshua Bengio. Generative adversarial nets. In *Advances in neural information processing systems*, pp. 2672–2680, 2014.

Kaiming He, Xiangyu Zhang, Shaoqing Ren, and Jian Sun. Deep residual learning for image recognition. *2016 IEEE Conference on Computer Vision and Pattern Recognition (CVPR)*, pp. 770–778, 2015.

Martin Heusel, Hubert Ramsauer, Thomas Unterthiner, Bernhard Nessler, and Sepp Hochreiter. Gans trained by a two time-scale update rule converge to a local nash equilibrium. In *Advances in Neural Information Processing Systems*, pp. 6626–6637, 2017.

Quan Hoang, Tu Dinh Nguyen, Trung Le, and Dinh Phung. MGAN: Training generative adversarial nets with multiple generators. In *International Conference on Learning Representations*, 2018. URL `https://openreview.net/forum?id=rkmu5b0a-`.

Xun Huang, Yixuan Li, Omid Poursaeed, John Hopcroft, and Serge Belongie. Stacked generative adversarial networks. In *The IEEE Conference on Computer Vision and Pattern Recognition (CVPR)*, July 2017.

Phillip Isola, Jun-Yan Zhu, Tinghui Zhou, and Alexei A Efros. Image-to-image translation with conditional adversarial networks. In *Proceedings of the IEEE conference on computer vision and pattern recognition*, pp. 1125–1134, 2017.

Y Jin, J Zhang, M Li, Y Tian, and H Zhu. Towards the high-quality anime characters generation with generative adversarial networks. In *Proceedings of the Machine Learning for Creativity and Design Workshop at NIPS*, 2017.

Tero Karras, Samuli Laine, and Timo Aila. A style-based generator architecture for generative adversarial networks. In *Proceedings of the IEEE Conference on Computer Vision and Pattern Recognition*, pp. 4401–4410, 2019.

Alex Krizhevsky et al. Learning multiple layers of features from tiny images. Technical report, Citeseer, 2009.

Karol Kurach, Mario Lučić, Xiaohua Zhai, Marcin Michalski, and Sylvain Gelly. A large-scale study on regularization and normalization in gans. In *International Conference on Machine Learning*, pp. 3581–3590, 2019.

Yann LeCun. The mnist database of handwritten digits. *http://yann. lecun. com/exdb/mnist/*, 1989.

Christian Ledig, Lucas Theis, Ferenc Huszár, Jose Caballero, Andrew Cunningham, Alejandro Acosta, Andrew Aitken, Alykhan Tejani, Johannes Totz, Zehan Wang, et al. Photo-realistic single image super-resolution using a generative adversarial network. In *Proceedings of the IEEE conference on computer vision and pattern recognition*, pp. 4681–4690, 2017.

Aravindh Mahendran and Andrea Vedaldi. Understanding deep image representations by inverting them. In *Proceedings of the IEEE conference on computer vision and pattern recognition*, pp. 5188–5196, 2015.

Takeru Miyato, Toshiki Kataoka, Masanori Koyama, and Yuichi Yoshida. Spectral normalization for generative adversarial networks. In *International Conference on Learning Representations*, 2018. URL `https://openreview.net/forum?id=B1QRgziT-`.

Mehdi S. M. Sajjadi, Olivier Bachem, Mario Lučić, Olivier Bousquet, and Sylvain Gelly. Assessing Generative Models via Precision and Recall. In *Advances in Neural Information Processing Systems (NeurIPS)*, 2018.

Karen Simonyan, Andrea Vedaldi, and Andrew Zisserman. Deep inside convolutional networks: Visualising image classification models and saliency maps. *arXiv preprint arXiv:1312.6034*, 2013.

Mukund Sundararajan, Ankur Taly, and Qiqi Yan. Axiomatic attribution for deep networks. In *Proceedings of the 34th International Conference on Machine Learning-Volume 70*, pp. 3319–3328. JMLR. org, 2017.

Christian Szegedy, Vincent Vanhoucke, Sergey Ioffe, Jon Shlens, and Zbigniew Wojna. Rethinking the inception architecture for computer vision. In *Proceedings of the IEEE conference on computer vision and pattern recognition*, pp. 2818–2826, 2016.

Ting-Chun Wang, Ming-Yu Liu, Jun-Yan Zhu, Guilin Liu, Andrew Tao, Jan Kautz, and Bryan Catanzaro. Video-to-video synthesis. *arXiv preprint arXiv:1808.06601*, 2018.

Chenshen Wu, Luis Herranz, Xialei Liu, Joost van de Weijer, Bogdan Raducanu, et al. Memory replay gans: Learning to generate new categories without forgetting. In *Advances In Neural Information Processing Systems*, pp. 5962–5972, 2018.

Fisher Yu, Yinda Zhang, Shuran Song, Ari Seff, and Jianxiong Xiao. Lsun: Construction of a large-scale image dataset using deep learning with humans in the loop. *arXiv preprint arXiv:1506.03365*, 2015.

Matthew D Zeiler and Rob Fergus. Visualizing and understanding convolutional networks. In *European conference on computer vision*, pp. 818–833. Springer, 2014.

Jun-Yan Zhu, Taesung Park, Phillip Isola, and Alexei A Efros. Unpaired image-to-image translation using cycle-consistent adversarial networks. In *Proceedings of the IEEE international conference on computer vision*, pp. 2223–2232, 2017.

## A Additional figures and experiments

### A.1 Ablation on number of blocks

Here we investigate the impact of the number of blocks in each RPGAN bucket on the generation quality. We train RPGAN with SN-ResNet backbone on CIFAR-10 with all hyperparameters fixed but with a varying number of blocks in buckets. For simplicity, all buckets have the same number of blocks. The resulting FID scores are presented on Figure 7

If the number of blocks is too low, the resulting latent space appears to have insufficient cardinality to cover the dataset. On the other hand, a too high number of blocks results in a difficult training procedure and also fails.

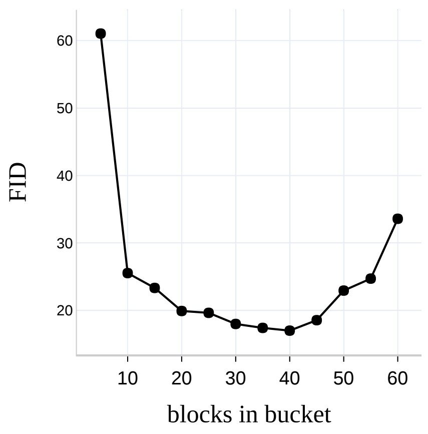

Figure 7: FID for RPGAN with different number of blocks.

### A.2 LSUN BEDROOM DATASET

To generate LSUN-bedroom-like images, we use the 7-bucket RPGAN with ResNet-like backbone model with five residual blocks, the first fully-connected layer, and the last convolutional layer. Similarly to CIFAR-10 experiments, during the generation, we freeze a random path and vary blocks in a single bucket to investigate its responsibility. See Figure 11 for blocks variations and Figure 12 for buckets responsibility analysis. Note that similarly to CIFAR-10, the central buckets have a maximal semantic impact. Last two buckets are mostly responsible for coloring. The first two buckets are responsible for local geometrical features. Note that here we face the mode collapse for the third bucket: mainly, it affects only tiny local features. See Figure 13 for samples generated by the model.

### A.3 ANIME FACES DATASET

Though this dataset is not standard for GANs, we use it in the experiments as it nicely reveals the RPGAN analysis tools. Here we use the 6-bucket RPGAN with ResNet-like backbone model with four residual blocks, the first fully-connected layer, and the last convolutional layer. See Figure 14 for blocks variations and Figure 15 for buckets responsibility analysis. Again, the content semantics is mostly defined by the intermediate buckets. Last two buckets are mostly responsible for coloring: the fifth bucket has the maximal impact on coloring, and the last bucket varies tones. The first buckets are responsible for small details (one can note the hair on the character's forehead). See Figure 16 for samples generated by the model.

| **Original** | **Compressed** |
|---|---|
| $z \in \mathbb{R}^{128}$ | |
| fc, 32 blocks, 128 | |
| fc, 32 blocks, 256 | |
| fc, 32 blocks, 512 | fc, 128 blocks, 784 |
| fc, 16 blocks, 1024 | |
| fc, 16 blocks, 784 | |
| Tanh, reshape to $28 \times 28$ | |

Table 3: Fully connected RPGAN without nonlinearities and its compressed modification.

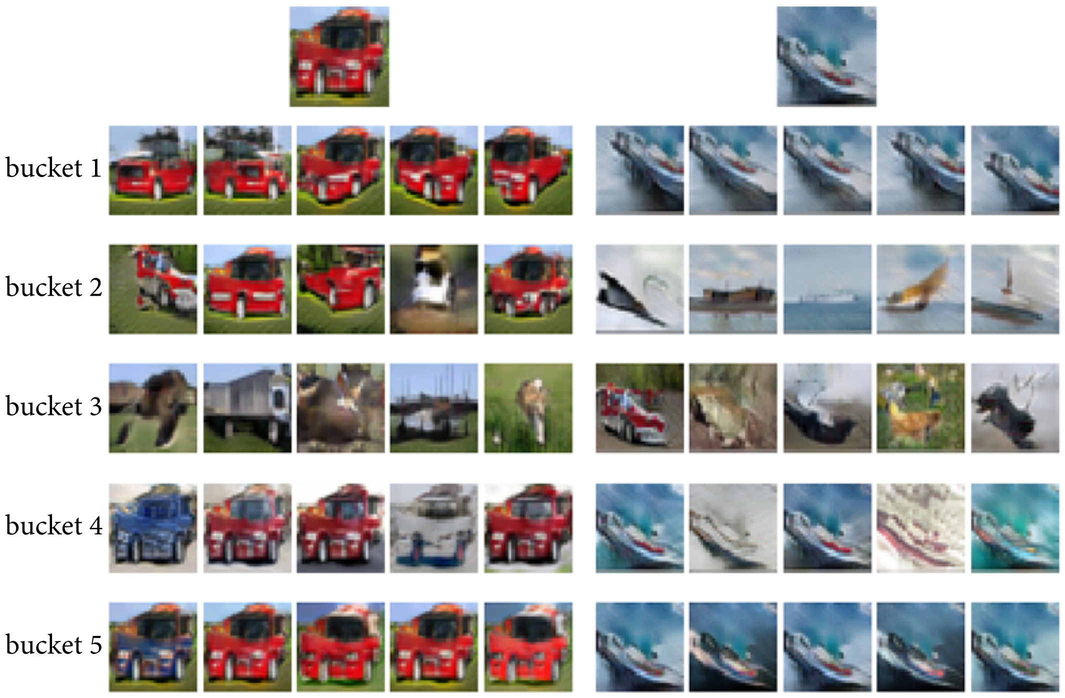

Figure 8: Freezed paths individual blocks variation in 5-bucket RPGAN.

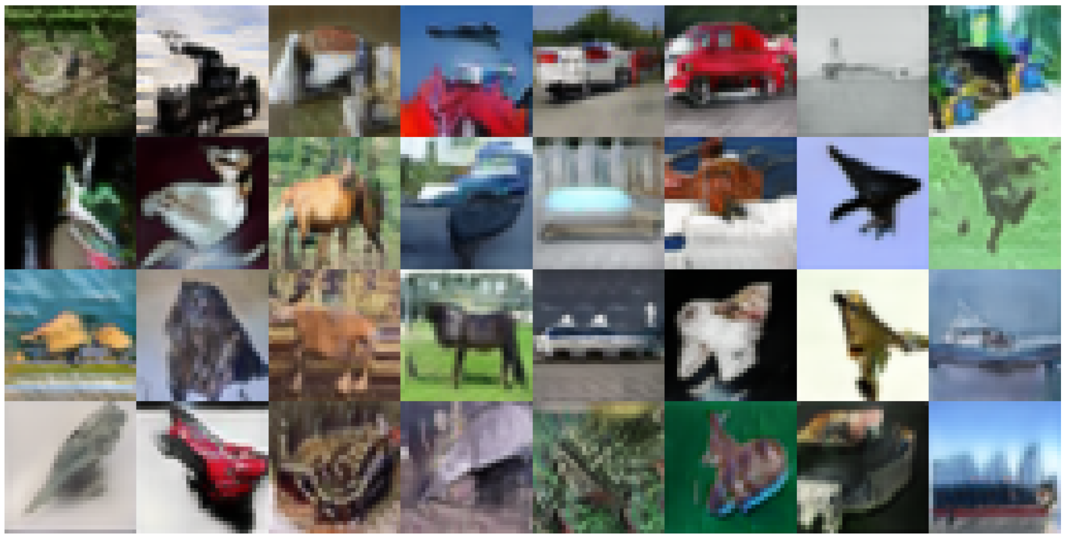

Figure 9: 32 $\times$ 32 samples generated by 5-bucket RPGAN.

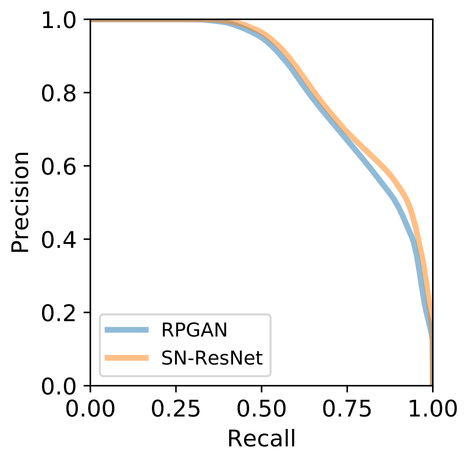

Figure 10: Comparison of precision-recall of RPGAN and its backbone SN-ResNet trained on CIFAR10.

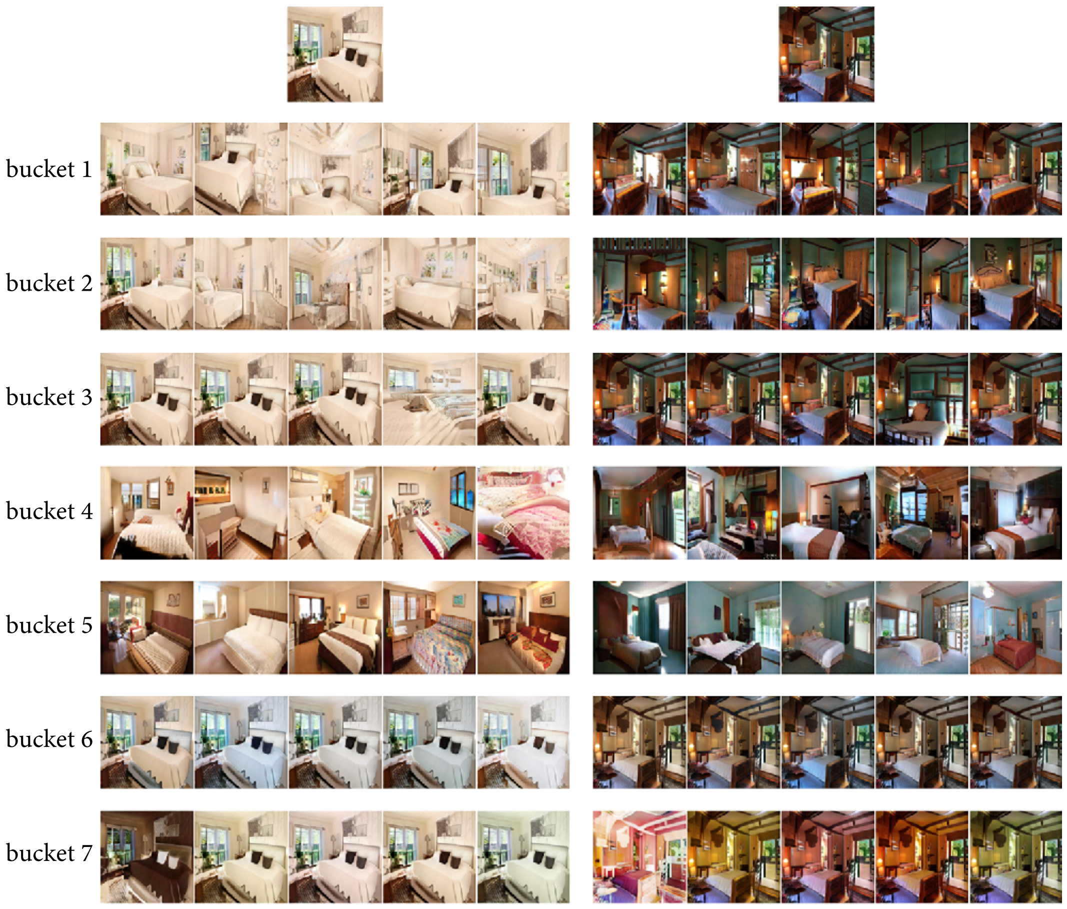

Figure 11: Freezed paths individual blocks variation in 7-bucket RPGAN.

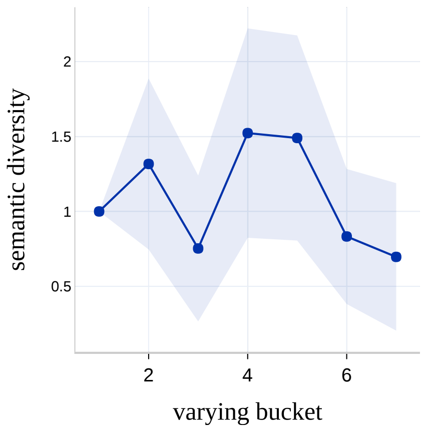

(a) Averaged relative inception impact

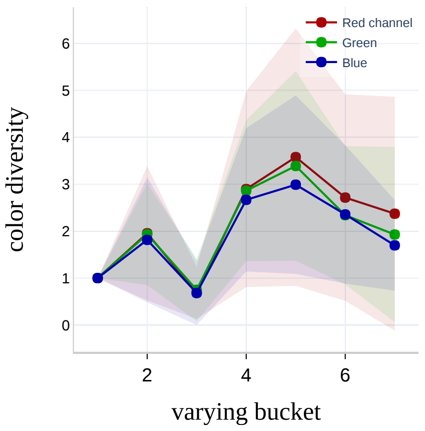

(b) Averaged relative coloring impact

Figure 12: LSUN bedroom buckets specification. See Section 4.1 for details.

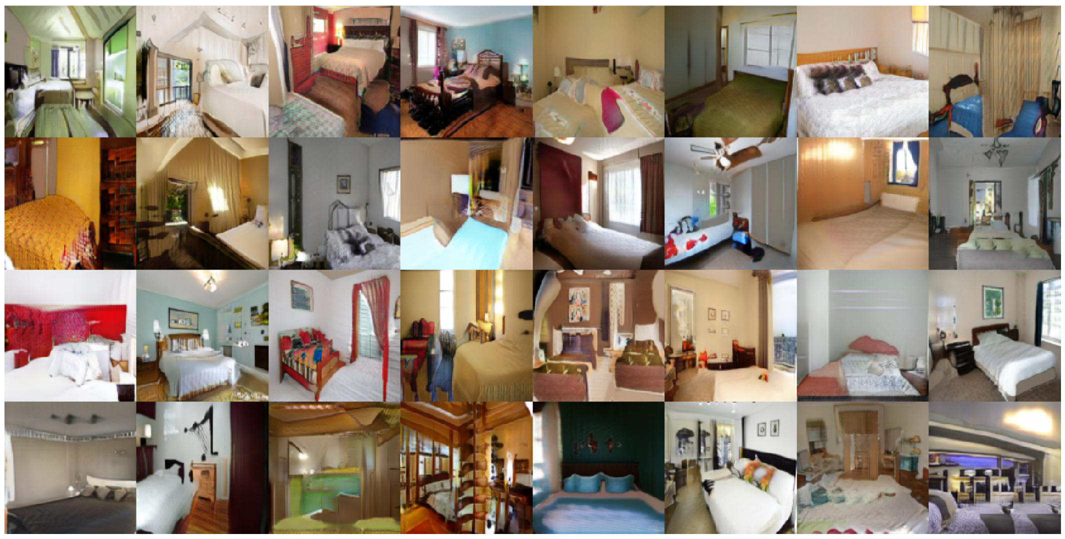

Figure 13: 128 × 128 samples generated by 7-bucket RPGAN

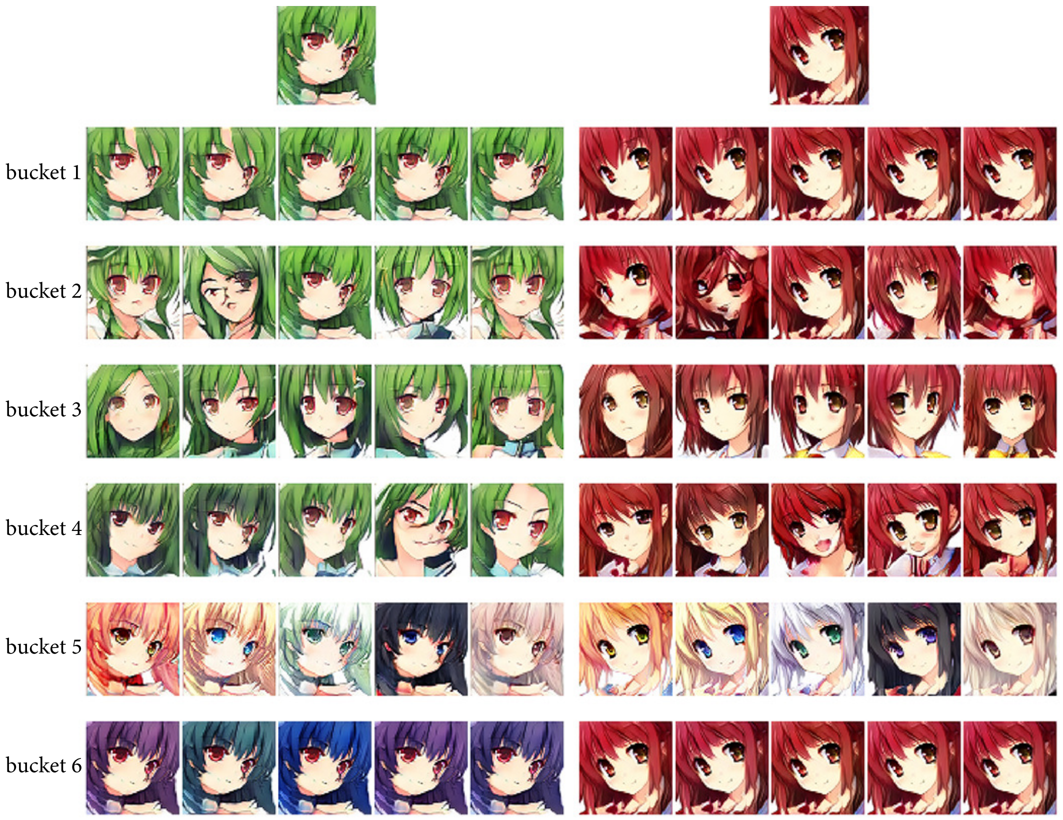

Figure 14: Freezed paths individual blocks variation in 6-bucket RPGAN.

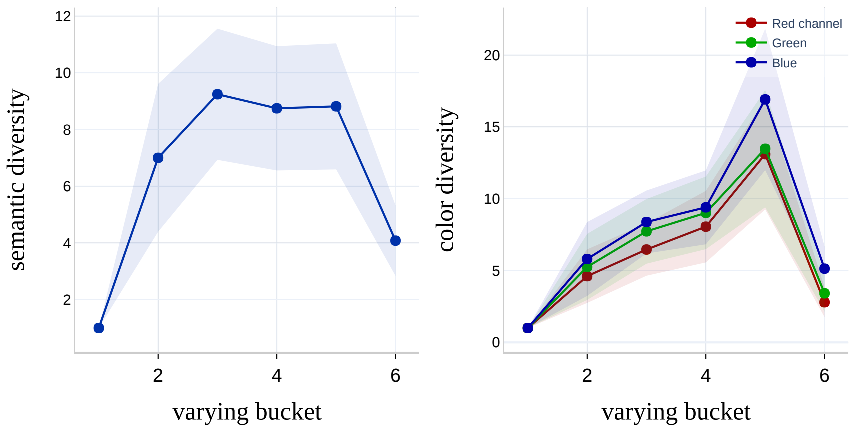

(a) Averaged relative inception impact (b) Averaged relative coloring impact

Figure 15: Anime Faces buckets specification. See Section 4.1 for details.

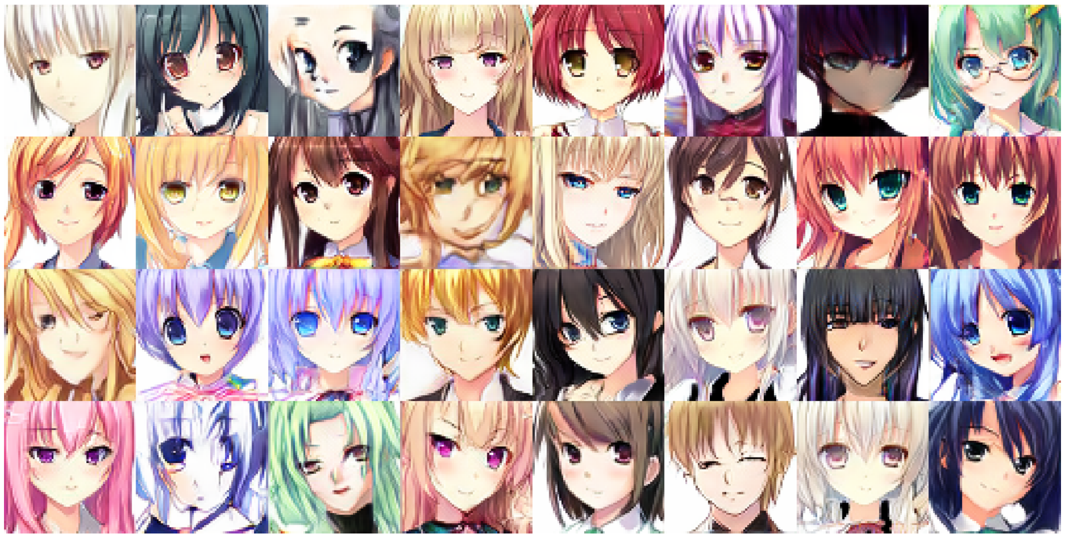

Figure 16: $64 \times 64$ samples generated by 6-bucket RPGAN.

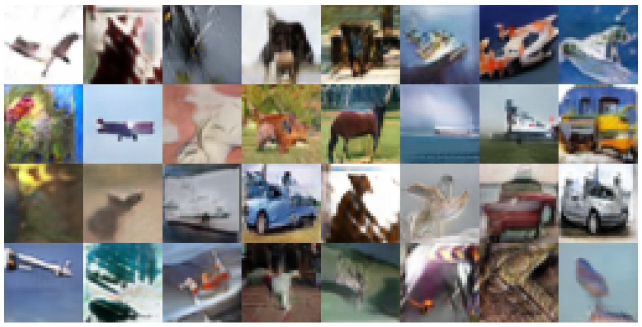

Figure 17: Samples from a 5-bucket ResNet-like generator without nonlinearities.

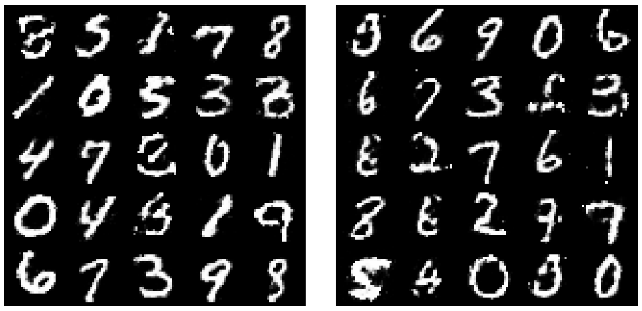

Figure 18: Digits generated by RPGAN without nonlinearities (*left*) and by its $\times 2.2$ faster compression (*right*).